Journal of
Nanoscience and Nanotechnology
Vol. 8, 6310–6315, 2008

The Relationship Between Internalization of Magnetic Nanoparticles and Changes of Cellular Optical Scatter Signal

Jingguang Xia[1], Song Zhang[1], Yu Zhang[1], Ming Ma[1], Kang Xu[1], Meng Tang[2], and Ning Gu[1,*]

[1] *Jiangsu Provincial Key Laboratory of Biomaterials and Devices, State Key Laboratory of Bioelectronics, School of Biological Science and Medical Engineering, Southeast University, Sipailou 2, Nanjing 210096, China*
[2] *School of Public and Health, Southeast University, Dingjiaqiao 87, Nanjing 210009, China*

Carboxylmethyl starch sodium-coated magnetic nanoparticles (CMS@MNs) with average size of 10 nm were synthesized by chemical coprecipitation. Cellular iron content showed that CMS@MNs could be efficiently uptaken by human hepatoma cells. TEM image showed that clusters consisting of nanoparticles were enclosed within sub-micrometric endosomes and one cell contained several such endosomes. After incubation with the nanoparticles, a phenomenon appeared that the intensity of cellular side scatter signal (SSC) obtained by flow cytometry at 488 nm argon laser increased. It was demonstrated that the increase of SSC signal was induced by a cell itself, and mainly caused by the nanoparticles both adsorbed on the membrane and internalized into cytoplasm. Although without inducing cell death the treatments with the nanoparticles could lead to increased permeability of cell membrane to propidium iodide. Results implied a potential that flow cytometry might be used as a tool to rapidly evaluate and select cells with high magnetic labeling and high viability in cellular transplant.

Keywords: Magnetic Nanoparticle, Endocytosis, Side Scatter Signal, Cell Viability, Magnetic Labeling.

1. INTRODUCTION

There are increasing explorations of magnetic iron oxide nanoparticles as MRI contrast agents, drug delivery systems, and thermoseeds for hyperthermia, all of which mainly utilize the special magnetic characteristics of this type of nanoparticles.[1–5] Sustained stability in physiological condition is the prerequisite for magnetic nanomaterials to be used in cellular and animal experiments. Additionally, both excellent biocompatibility and bio-functionality are also important aspects that determine whether they could be used in biomedicine. To achieve these ends, various strategies have been carried out to decorate magnetic iron oxide nanoparticles. Surface modification with polymers can avoid the precipitation by steric hindrance effect, among of which PEGylation (modified with poly(ethylene glycol)) is widely employed because of its biocompatibility and convenience for subsequent conjugation with biological molecules.[6–9] Non-polymer surface modifications, such as *meso*-2,3-dimercaptosuccinic acid, have also been used to yield magnetic nanoparticles stable in physiological condition.[10]

For most applications, relatively large amounts of nanoparticles should be delivered into cells and targeting specificity is also necessary. For example, to efficiently track the transplanted stem cells and other mammalian cells used in cellular therapy, HIV-tat peptides, protamine, and other transfection agents have been adopted to facilitate the internalization of iron oxide nanoparticles into these cells.[11–14] The conjugation with folate or methotrexate could realize specific targeting of iron oxide nanoparticles to tumor cells over-expressing folate receptor and subsequent endocytosis of nanoparticles, as could improve the MRI or drug delivery in target organs.[9, 15, 16] Superparamagnetic iron oxide nanoparticles attached with specific proteins, antibodies, peptides could be used to efficiently image the sites of inflammation, neovasculature, apoptosis or tumor.[17–19] When derivatized with carbohydrates containing galactose, iron oxide nanoparticles were selectively accumulated in hepatocytes after injection, indicating a potential application for drug targeting delivery.[20] Besides the specific targeting and uptake of magnetic nanoparticles modified with various ligands, non-specific but high levels of uptake occurs between some types of cells and magnetic nanoparticls.[21–23]

*Author to whom correspondence should be addressed.

 1533-4880/2008/8/6310/006 doi:10.1166/jnn.2008.355

To evaluate the internalized efficacy of magnetic nanoparticles or the cellular targeting specificity, a widely used method is to incorporate fluorescent substances into nanoparticles, such as quantum dots (QDs) and fluorescent dyes. The quantity of adsorption or internalization of the nanoparticles could be indirectly reflected from the intensity of fluorescence measured by fluorescent microscope or flow cytometry.[11, 13, 24] However, the cytotoxicity of QDs and the easily bleachable fluorescence of dyes make their practical applications uncertain.[25, 26] Moreover, the introduction of QDs and dyes makes the synthesis of nanoparticles more complex. Therefore, other method is also required.

Very recently, the work of Suzuki et al.[27] showed that the intensity of side-scattered light could reflect uptake potential of nanosized particles. In this work, using magnetic nanoparticles coated with carboxylmethyl starch sodium (noted CMS@MNs) and human hepatoma cells SMMC-7721, we also found that the relative quantity of internalized nanoparticles could be indirectly reflected from the intensity of side scatter signal obtained by flow cytometry. And our results further demonstrated that the increase of SSC is mainly caused by the nanoparticles both adsorbed on the cell surface and enclosed within endosomes. Results also implied the possibility of flow cytometry as a convenient tool to evaluate the efficacy of magnetic labeling and the viability of labeled cells.

2. MATERIALS AND METHODS

2.1. The Synthesis and Characterization of CMS@MNs

CMS-coated magnetite nanoparticles were synthesized by chemical coprecipitation based on literature.[28] Carboxylmethyl starch sodium was dissolved in deionized water at 80 °C under magnetic stirring. An iron solution containing $FeCl_3$ and $FeSO_4$ (molar ratio 2:1) was prepared under N_2 protection. A mixture of iron and CMS solution was prepared (vol. ratio 1:4) under vigorous stirring, and then enough ammonia aqueous solution was added dropwise with violently stirring at 60 °C for 2 h. After the reaction, the remaining solution was cooled to room temperature. The yielding CMS-coated magnetite nanoparticles were dialyzed to remove the unreacted CMS and ions at 37 °C for 2–3 days against distilled water that replaced every day. Scanning electron microscope (Sirion-2000, FEI Company) was used to characterize the morphology of CMS@MNs after the samples were deposited on silicon substrates and sprayed with gold.

2.2. Cell Culture and Treatments

Human hepatoma cell line, SMMC-7721 was generously donated by Institute of Cardiovascular Disease, Nanjing Medical University, China. Cells were cultured in RPMI 1640 medium containing 10% fetal calf serum, 100 U/ml penicillin and 100 μg/ml streptomycin at 37 °C in 5% CO_2. Nanoparticles were directly dissolved in medium containing serum because of their excellent stability. In experiments, cells were grown in plates for 24 h before incubation with nanoparticles.

2.3. Cellular Uptake of CMS@MNs

Iron content in cells was measured using potassium thiocyanate method. The same number of cells were seeded in 6-well plates and grown for about 24 h. Then to the original medium CMS@MNs suspension was added, yielding final iron concentration of 1 mM. After further incubation for different time, the cells were thoroughly washed with phosphate-buffered solution (PBS), and trypsinized. The detached cells were completely dissolved in 0.2 ml of concentrated HCl at 60 °C for 2 h. After the lysates cooled down to room temperature, 0.2 ml of 5% trichloroacetic acid was added. Then 4.25 ml of the reagent of potassium thiocyanate (composed of 2.5 ml ddH_2O, 0.25 ml concentrated HCl, 0.5 ml 2% $K_2S_2O_6$ and 1 ml 20% NH_4SCN) was added. The absorbance at 490 nm was read using Bio-Rad microplate reader (model 680) and iron content was calculated according to a standard curve of $FeSO_4$

The TEM samples of cells were prepared as described below. Following the incubation with the same concentration of CMS@MNs for 24 h, cells were washed with PBS for 3 times, harvested and fixed with 4% glutaraldehyde in 4 °C. Then the cells were post-fixed in 1% osmium tetraoxide for 30 min. After washed with PBS three times, the samples were dehydrated with graded solutions of acetone (30%, 50%, 70%, 80%, 90%, and 100%) for 10 min in each solution. After dehydration, the samples were treated with increased ratio of embedding agent to acetone (from 1:1, 2:1 to pure embedding agent) for 1 h for each step, and then processed in molds at 60 °C. Ultrathin sections of 70 nm were cut, first stained with uranyl acetate, then stained with lead nitrate, and finally viewed under a Hitachi electron microscope (H-600) at 80 kv.

2.4. Side Scatter Signal Obtained by Flow Cytometry

During the detection of the viability of magnetic nanoparticles-incubated cells using flow cytometry, we observed that their side scatter signal (SSC) changed evidently. Thus, experiments were designed to demonstrate the effects that magnetic nanoparticles interacting with cells had on SSC signal obtained by flow cytometry at 488 nm argon-ion laser (BD FACSCalibur). Cells were treated as described below:

(1) cells were incubated with CMS@MNs ([Fe = 1 mM]) for different time, then SSC was detected,

(2) Cells were first incubated with different concentrations of CMS@MNs for 24 h, then cultured in nanoparticle-free medium for additional 48 h, at last SSC was detected,

(3) Cells were first incubated with different concentrations of CMS@MNs for 24 h, then reseeded and cultured for different time, at last SSC was detected.

For SSC detection, cells were thoroughly washed with PBS to remove nanoparticles, harvested and prepared into single cell suspension, and then loaded to flow cytometry. At least 10^5 cells were tested for each sample. For data analysis, the value of SSC intensity was divided into four regions: M1 (0–200), M2 (200–400), M3 (400–600), and M4 (600–800).

2.5. Cell Viability

Propidium iodide (PI) staining was used to assess cell viability after incubation with CMS@MNs. The same quantity of cells was plated in 6-well plates and cultured for 24 h, and then nanoparticle-containing medium was added. After incubation in the same condition for another 24 h, the cells were washed with PBS to thoroughly remove particles, harvested, and then washed with PBS. For flow cytometry analysis, the cells were dissolved in 0.3 ml of PI solution (final concentration is 10 μg/ml) and placed in dark for 20 min. At least 10^5 cells were tested for each sample. For data analysis, the value of FL-2 (PI) intensity was divided into three regions: M1 (0–10^1), M2 (10^1–10^2) and M3 (>10^2). Apparently, dead cells were located in the region of M1.

3. RESULTS

3.1. The Characteristic of CMS@MNs

Figure 1 shows the SEM image of CMS-coated magnetic nanoparticles with very homogeneous size distribution. Through calculation, the average size is 10 nm. It can be said that the agglomeration of nanoparticles in SEM image is the result of dryness during the sample preparation, because CMS@MNs exhibit excellent stability in aqueous solution.

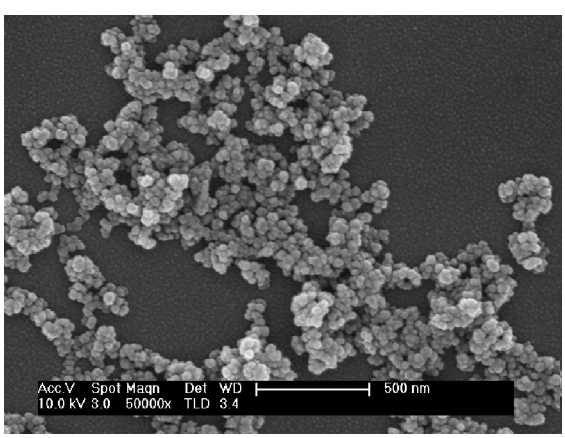

Fig. 1. SEM image of CMS@MNs.

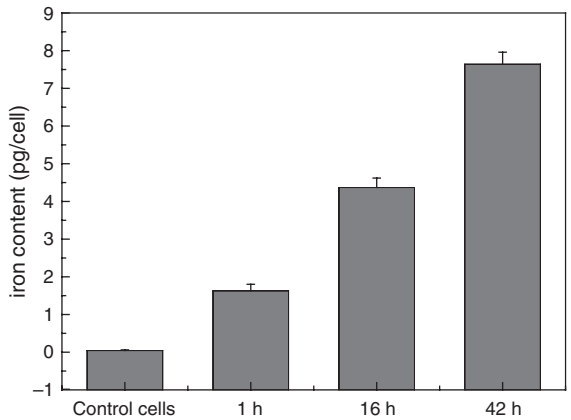

Fig. 2. Iron content in cells after incubation with CMS@MNs (1 mM of iron) for different time.

3.2. Cellular Uptake of CMS@MNs

After incubation, most of magnetic nanoparticls can be removed by washing with PBS because of their perfect stability in medium. Thus, the quantity of iron tested could match that adsorbed and incepted by cells. In contrast to almost undetectable iron in control cells, iron content came to 1.6, 4.3, and 7.6 pg/cell, respectively after incubation with nanoparticles for 1, 16, and 42 h, revealing

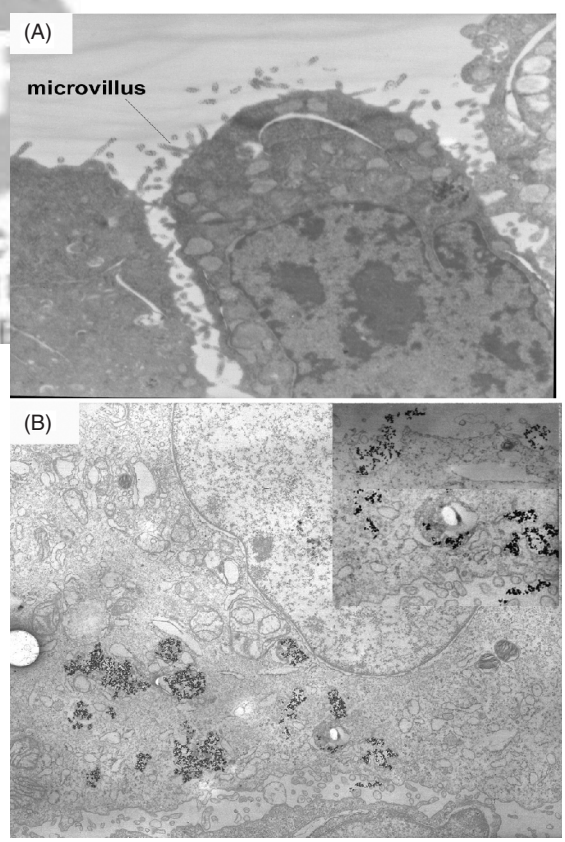

Fig. 3. TEM images of cells after incubation with CMS@MNs (1 mM of iron) for 24 h. (A) control cell, (B) treated cell, and an endocytic vesicle in process (inset).

actively endocytosis of CMS@MNs by hepatoma cells (Fig. 2). TEM images showed that on the hepatoma cell surface, there are a lot of microvilli (Fig. 3(A)), an important ultrastructure of tumor cells distinguished from normal cells. These microvilli maybe play an important role in the adsorption and subsequent endocytosis for nanoparticles. Figure 3(B) showed that clusters of magnetic nanoparticles were internalized into endosomes and usually, one cell contained several such endosomes with different sizes. There are also clusters formed from nanoparticles on the cell surface (Fig. 3(B), inset) that could partly contribute to the iron content tested. Consequently, it is conceivable that cellular iron content tested here came from the nanoparticles both adsorbed on cell surface and internalized into cells.

3.3. Side Scatter Signal Obtained by Flow Cytometry

Side scatter signal reflects the density and granularity of a cell, higher density and more granules with stronger SSC signal. Forward scatter signal (FSC) reflects the size of a cell, which can differentiate live cells from necrotic cells with smaller size. After incubation with nanoparticles, the mean intensity of FSC almost did not change compared with control cells, showing that cells could keep their sizes during the absorption of nanoparticles (histograms not shown), however, the intensity of SSC increased evidently (Fig. 4). With the prolongation of incubation time, the percentage of cells in the region of M1 (low signal intensity) decreased significantly, resulting in corresponding increase of cells in the regions of M2 and M3

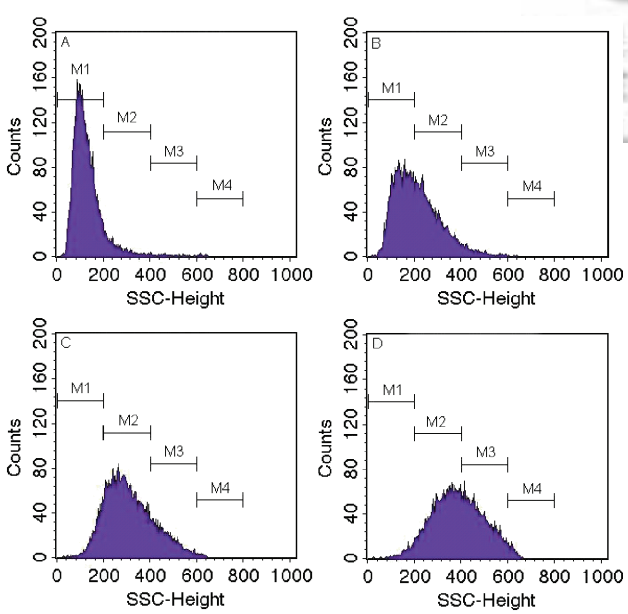

Fig. 4. Side scatter signal of cells detected by flow cytometry (488 nm Argon laser) after incubation with CMS@MNs suspension (1 mM of iron). (A) Control cells, (B, C, D) incubation with nanoparticles for 1, 16, 42 h, respectively.

Table I. Side scatter signal of hepatoma cells after incubation with CMS@MNs ([Fe] = 1 mM) for different time.

		Incubation time (h)		
SSC intensity	Control cells	1	16	42
M1 (0–200)	80.1 ± 4.4	55.5 ± 1.2	13.5 ± 0.8	2.6 ± 0.5
M2 (200–400)	14.3 ± 4.2	41.9 ± 1.0	70.4 ± 0.4	56.1 ± 1.2
M3 (400–600)	0.8 ± 0.3	2.9 ± 0.3	16.3 ± 1.1	40.4 ± 0.5
M4(600–800)	0.01 ± 0	0.04 ± 0.02	0.3 ± 0.1	1.5 ± 0.2
Mean	141.0 ± 9.1	202.4 ± 2.3	302.6 ± 3.2	381.9 ± 0.7

(high signal intensity) (Table I). For cells incubated for 1, 16, and 42 h, the mean intensity of SSC are 202, 302, and 381, respectively, showing significant increase compared to 140 of control cells (Table I). The results indicated that nanoparticles interacting with cells could strengthen cellular SSC signal intensity. To further examine the relationship between nanoparticles interacting with cells and the intensity of SSC signal, two experiments were conducted. In one experiment, nanoparticles was used to incubate cells for 24 h, and then removed, and after further incubation in nanoparticle-free medium for 48 h, the intensity of SSC was detected. The results showed that SSC signal intensity decreased after the removing of nanoparticles, and especially for cells incubated with low concentration of nanoparticles ([Fe] = 0.5 mM), their SSC signal intensity decreased close to that of control cells (Table II). In the other experiment, the cells were first incubated for 24 h, and then reseeded, and 24 h or 72 h following reseeding SSC signal was detected. The results showed that 24 h following reseeding SSC intensity decreased slightly, while 72 h following reseeding the intensity decreased drastically, reaching to the level similar with control cells (Table III). Results above indicated that the intensity of SSC signal decreased rapidly with the reduction of intracellular nanoparticles due to cell division, implying that SSC intensity could reflect the relative content of intracellular nanoparticles.

3.4. Viability

PI staining was used to evaluate the viability of cells because PI is not permeable for the membrane of vital cells, but permeable for membrane of necrotic cells. After incubation with magnetic nanoparticles containing 0.5, 1

Table II. Side scatter signal of hepatoma cells after incubation with CMS@MNs for 24 h, and 48 h in nanoparticle-free medium.

		Nanoparticles concentration (mM iron)		
SSC intensity	Control cells	0.5	1	2
M1 (0–200)	81.5 ± 1.2	77.2 ± 0.1	60.6 ± 0.4	40.3 ± 0.4
M2 (200–400)	17.7 ± 1.0	22.4 ± 0.1	37.5 ± 0.4	53.9 ± 2.8
M3 (400–600)	1.0 ± 0.2	0.7 ± 0.04	2.4 ± 0.02	6.0 ± 1.0
M4(600–800)	0.01 ± 0	0.02 ± 0.01	0.02 ± 0.01	0.1 ± 0.03
Mean	144.9 ± 4	161.1 ± 1.0	195.0 ± 1.0	237.7 ± 7.4

Table III. Side scatter signal of hepatoma cells from reseeded and cultured cells that were incubated with CMS@MNs for 24 h.

		Nanoparticles concentration (mM iron)			
		24 h following passage		72 h following passage	
SSC intensity	Control cells	1	2	1	2
M1 (0–200)	81.5±1.2	46.7±0.3	29.2±0.2	81.6±3.3	87.8±2.9
M2 (200–400)	17.7±1.0	51.0±0.4	65.0±0.1	18.1±3.1	12.1±2.9
M3 (400–600)	1.0±0.2	3.0±0.1	6.4±0.1	0.7±0.3	0.3±0.1
M4(600–800)	0.01±0	0.02±0	0.1±0.03	0.01±0	0.01±0
Mean	144.9±4	219.6±0.2	254.9±0.2	149.1±6.9	138.4±3.8

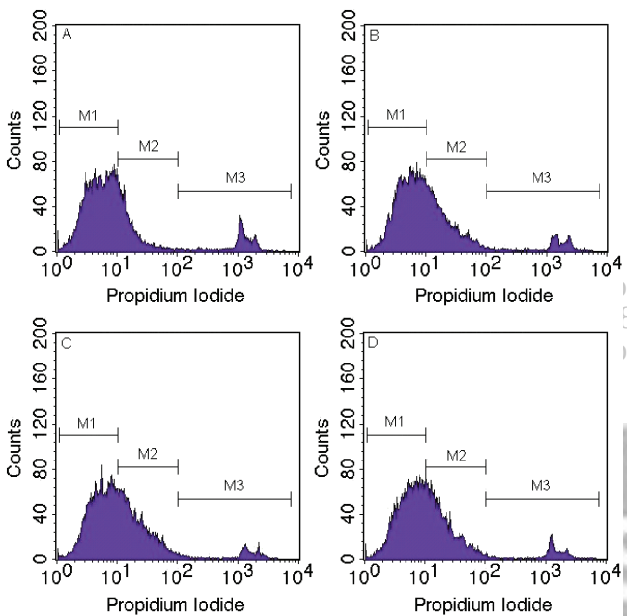

Fig. 5. Histograms of FL-2 (PI) of CMS@MNs-incubated cells obtained by flow cytometry after PI-staining. (A) Control cells, (B, C and D) cells incubated with nanoparticles (0.5, 1 and 2 mM of iron) for 24 h.

and 2 mM of iron for 24 h, the percentages of dead cells with FL-2 intensity located in the region of M3 are 5.52%, 4.69%, and 6.17%, respectively, and the values did not increase compared with 8.43% of control cells. However, the percentages of cells with stronger PI staining (cells in the region of M2) increased significantly, from 11.5±1.1% of control cells to 32.8±0.8%, 38.0±% and 38.7±0.7% of treated cells (Fig. 5 and Table IV). The results indicated that although without inducing cell death the treatments with magnetic nanoparticles could lead to increased permeability of cell membrane to PI.

Table IV. PI staining of hepatoma cells after incubation with CMS@MNs for 24 h.

		Nanoparticles concentration (mM iron)		
Fluorescence intensity	Control cell	0.5	1	2
M1($0–10^1$)	78.8±1.1	62.1±1.2	57.6±2.5	55.4±0.2
M2 ($10^1–10^2$)	11.5±1.1	32.8±0.8	38.0±2.6	38.7±0.7
M3 ($10^2–10^3$)	8.4±0.3	5.5±0.3	4.7±0.1	6.2±0.9

4. DISCUSSION

Because of their ability as MRI contrast agents to localize the labeled stem cells or other cells after transplantation, many efforts are devoted to prepare superparamagnetic iron oxide nanoparticles that could be non-specifically but readily captured by cells. Based on observations on anionic iron oxide nanoparticles, non-specific endocytosis could be modeled as a two-step process: first binding at the cell membrane and forming clusters, described as a Langmuir adsorption, and subsequent internalization through invagination of plasma membrane.[29] After internalization, iron oxide nanoparticles were concentrated into endosomes or lysosomes where they were retained for several days.[22, 30] Here, human hepatoma cells exhibited adsorption endocytosis with relatively large quantities for CMS@MNs, as demonstrated by iron content detection. In cells, there are many sub-micrometric endosomes with different sizes each enclosing lots of iron oxide particles. It is well-known that the characters of tumor cells in biology, biochemistry, and molecular biology are very different from that of normal cells, among of which the changes of surface ultrastructure and membrane molecules expression are associated with adhesion, recognition, and signal transduction. These changes might be also associated with more absorption of magnetic nanoparticles by tumor cells than normal cells. Here, TEM image shows that on the surface of tumor cells there are lots of microvilli (Fig. 3(A)) which could largely increase the membrane area that determines the number of nanoparticles adsorbed. Moreover, very possibly, microvilli play a role in the formation of nanoparticle clusters on the membrane that would be endocytosed by cells subsequently (Fig. 3(B), inset).

Results above showed that nanoparticles interacting with cells consisted of two parts: nanoparticles in the form of clusters adsorbed on cell surface and nanoparticles concentrated into endosomes. In combination with the fact that nanoparticles-incubated cells presented high intensity of SSC signal, it could be concluded that these two parts of nanoparticles together led to the alterations of SSC signals intensity. With the prolongation of incubation time, both intracellular iron content and SSC signal intensity increased evidently, and with the cell division SSC intensity decreased rapidly. These results suggested that the signal intensity could indirectly reflect the relative quantity of

nanoparticles absorbed by cells. The relationship between SSC intensity and cellular magnetic nanoparticles implied that flow cytometry might be used as a convenient and fast tool to evaluate cellular uptake of nanoparticles, especially for work involving lots of tests between nanoparticles with different coatings and different cell lines. For example, Weissleder et al.[31] synthesized a library comprising 146 magnetic nanoparticles decorated with different small molecules, and screened the library against different cell lines to discover nanoparticles with high affinity for specific cell types using fluorescent microscopy or fluorescence-activated cell sorting (FACS) analysis. If using the method of side-scatter light, the tests will be time and cost efficient.

In addition, flow cytometry can be used to assess cell viability or apoptosis readily and rapidly after staining with dyes, such as propidium iodide, 7-aminoactinomycin D (7-AAD), and Annexin V/FITC. Consequently, in combination with both viability and SSC signal intensity measurements, it is possible to evaluate the ability of cells to uptake magnetic nanoparticles and their viability or apoptosis simultaneously. Moreover, if flow cytometry is equipped with sorting modality, it will be helpful for selecting highly magnetic labeled and highly viable cells for cell transplant or other usages.

5. CONCLUSION

At present, fluorescent labeling is widely used to assess the uptake of magnetic nanoparticles by cells. However, the introduction of QDs and dyes might alter the property of nanoparticles in physiological solutions and provoke adverse effects on cells. In this study, we demonstrated that carboxylmethyl starch sodium coated magnetic nanoparticles could be efficiently absorbed by human hepatoma cells where clusters of nanoparticles were adsorbed on cell membrane or wrapped into endosomes with different sizes. We also demonstrated that clusters composed of nanoparticles could result in the increase of SSC signal intensity and suggested a simple and rapid method to evaluate nanoparticles uptake and cell viability by flow cytometry simultaneously.

Acknowledgments: This work is supported by grants from the National Natural Science Foundation of China (NSFC, 60571031, 90406023, 90406024, 60501009) and the National Basic Research Program of China (2006CB933206, 2006CB705600).

References and Notes

1. D. L. J. Thorek, A. K. Chen, J. Czupryna, and A. Tsourkas, *Biomed. Eng.* 34, 23 (**2006**).
2. T. K. Jain, M. A. Morales, S. K. Sahoo, D. L. Leslie-Pelecky, and V. Labhasetwar, *Molecular Pharmaceutics* 2, 194 (**2005**).
3. S. Takeda, B. Terazono, F. Mishima, H. Nakagami, S. Nishijima, and Y. Kaneda, *J. Nanosci. Nanotechnol.* 6, 3269 (**2006**).
4. I. Hilger, A. Kießling, E. Romanus, R. Hiergeist, R. Hergt, W. Andrä, M. Roskos, W. Linss, P. Weber, W. Weitschies, and W. A. Kaiser, *Nanotechnology* 15, 1027 (**2004**).
5. C. Wilhelm, J. P. Fortin, and F. Gazeau, *J. Nanosci. Nanotechnol.* 7, 2933 (**2007**).
6. J.-F. Lutz, S. Stiller, A. Hoth, L. Kaufner, U. Pison, and R. Cartier, *Biomacromolecules* 7, 3132 (**2006**).
7. N. Nitin, L. E. W. Laconte, O. Zurkiya, X. Hu, and G. Bao, *J. Biol. Inorg. Chem.* 9, 706 (**2004**).
8. A. K. Gupta and A. G. Curtis, *J. Mater. Sci.-Mater. M* 15, 493 (**2004**).
9. Y. Zhang, C. Sun, N. Kohler, and M. Zhang. *Biomedical Microdevices* 6, 33 (**2004**).
10. N. Fauconnier, J. N. Pons, J. Roger, and A. Bee, *J. Colloid Interf. Sci.* 194, 427 (**1997**).
11. L. Josephson, C. H. Tung, A. Moore, and R. Weissleder, *Bioconjugate Chem.* 10, 186 (**1999**).
12. A. S. Arbab, G. T. Yocum, H. Kalish, E. K. Jordan, S. A. Anderson, A. Y. Khakoo, E. J. Read, and J. A. Frank, *Blood* 104, 1217 (**2004**).
13. F. Reynolds, R. Weissleder, and L. Josephson, *Bioconjugate Chem.* 16, 1240 (**2005**).
14. A. S. Arbab, L. A. Bashaw, B. R. Miller, E. K. Jordan, B. K. Lewis, H. Kalish, and J. A. Frank, *Radiology* 229, 838 (**2003**).
15. F. Sonvico, S. Mornet, S. Vasseur, C. Dubernet, D. Jaillard, J. Degrouard, J. Hoebeke, E. Duguet, P. Colombo, and P. Couvreur, *Bioconjugate Chem.* 16, 1181 (**2005**).
16. N. Kohler, C. Sun, J. Wang, and M. Zhang, *Langmuir* 21, 8858 (**2005**).
17. D. E. Sosnovik, E. A. Schellenberger, M. Nahrendorf, M. S. Novikov, T. Matsui, G. Dai, F. Reynolds, L. Grazette, A. Rosenzweig, R. Weissleder, and L. Josephson, *Magn. Reson. Med.* 54, 718 (**2005**).
18. K. A. Kelly, J. R. Allport, A. Tsourkas, V. R. Shinde-Patil, L. Josephson, and R. Weissleder, *Circ. Res.* 96, 327 (**2005**).
19. O. Veiseh, C. Sun, J. Gunn, N. Kohler, P. Gabikian, D. Lee, N. Bhattarai, R. Ellenbogen, R. Sze, A. Hallahan, J. Olson, and M. Zhang, *Nano Lett.* 5, 1003 (**2005**).
20. K. M. K. Selima, Y. S. Ha, S. J. Kim, Y. Chang, T. J. Kim, G. H. Lee, and I. K. Kang, *Biomaterials* 28, 710 (**2007**).
21. C. Wilhelm, C. Billotey, J. Roger, J. N. Pons, J.-C. Bacri, and F. Gazeau, *Biomaterials* 24, 1001 (**2003**).
22. C. Billotey, C. Wilhelm, M. Devaud, J. C. Bacri, J. Bittoun, F. Gazeau, *Magn. Reson. Med.* 49, 646 (**2003**).
23. K. Schulze, A. Koch, A. Petri-Fink, B. Steitz, S. Kamau, M. Hottiger, M. Hilbe, L. Vaughan, M. Hofmann, H. Hofmann, and B. von Rechenberg, *J. Nanosci. Nanotechnol.* 6, 2829 (**2006**).
24. A. Hoshino, K. Hanaki, K. Suzuki, and K. Yamamoto, *Biochem. Bioph. Res. Co.* 314, 46 (**2004**).
25. A. O. Choi, S. J. Cho, J. Desbarats, J. Lovrić, and D. Maysinger. *J. Nanobiotechnology* 5, 1 (**2007**).
26. W.-H. Chan, N.-H. Shiao, and P.-Z. Lu, *Toxicol. Lett.* 167, 191 (**2006**).
27. H. Suzuki, T. Toyooka, and Y. Ibuki, *Environ. Sci. Technol.* 41, 3018 (**2007**).
28. D. K. Kim, M. Mikhaylova, F. H. Wang, J. Kehr, B. Bjelke, Y. Zhang, T. Tsakalakos, and M. Muhammed, *Chem. Mater.* 15, 4343 (**2003**).
29. C. Wilhelm, F. Gazeau, J. Roger, J. N. Pons, and J.-C. Bacri, *Langmuir* 18, 8148 (**2002**).
30. K. Müller, J. N. Skepper, M. Posfai, R. Trivedi, S. Howarth, C. Corot, E. Lancelot, P. W. Thompson, A. P. Brown, and J. H. Gillard, *Biomaterials* 28, 1629 (**2007**).
31. R. Weissleder, K. Kelly, E. Y. Sun, T. Shtatland, and L. Josephson, *Nat. Biotechnol.* 23, 1418 (**2005**).

Received: 23 November 2007. Accepted: 25 February 2008.